The Astrophysical Journal, 674:1144–1152, 2008 February 20

EVIDENCE OF RELENTLESS RECONNECTIONS AT BOUNDARIES OF SUPERGRANULAR NETWORK LANES IN QUIET SUN AND CORONAL HOLE

T. Aiouaz
High Altitude Observatory, National Center for Atmospheric Research, P.O. Box 3000, Boulder, CO 80307-3000; aiouaz@ucar.edu
Received 2007 July 2; accepted 2007 September 24

ABSTRACT

Doppler-shift properties of the solar transition region (TR) and low corona are investigated in relation to the underlying chromospheric supergranular network, with particular regard to the role of the magnetic field. EUV line properties were obtained from a large raster scan of the solar chromosphere, transition region, and corona acquired by the SUMER spectrometer on board *SOHO*. The observed region includes an equatorial coronal hole, as well as surrounding quiet-Sun areas. The chromospheric supergranular network pattern is enhanced using a filter defined previously by Aiouaz and coworkers applied to a Lyman continuum image. The filtered continuum image and Dopplergrams are used to produce dispersion plots. We find correlations between the chromospheric network, and the N IV (765.15 Å), O IV (790.19 Å), S V (786.50 Å), O V (760.45 Å) Doppler shifts in quiet Sun *and* coronal hole. It is established that the maximum inflow (redshift) at transition region temperatures appears statistically toward the center of the network lanes in the quiet-Sun areas and toward the boundary of the network lanes in the coronal hole. Furthermore, while the strong redshifts in the TR lines complement spatially blueshifts from the low corona (Ne VIII 770.41 Å) in a puzzle-like pattern, bidirectional flows (i.e., cospatial strong red- and blueshifts in the TR/Corona) appear predominantly in the coronal hole. The bidirectional flows congregate almost systematically at boundaries of magnetic field concentrations seen in *SOHO* MDI magnetograms. These results support a coherent interpretation of almost 30 years of unexplained statistical Doppler-shift variations in the transition region and corona for quiet Sun *and* coronal hole. The proposed scenario involves reconnections between the strong network magnetic field and continuously advected weak field from the supergranular cell interior.

Subject heading: Sun: corona

Online material: color figures

1. INTRODUCTION

The supergranular network is the pattern of supergranulation cells seen over the entire surface of the Sun outside of sunspots (Leighton et al. 1962). The magnetic field in the solar atmosphere is anchored in intense magnetic elements in the photosphere. Plasma flows in the photospheric layers carry the magnetic field to the edges of the supergranular convection cells, resulting in a larger magnetic flux in cell boundaries than in their interiors. The magnetic field expands higher up into the atmosphere through the transition region (TR) to fill the whole volume until it has become relatively uniform at the coronal level (Gabriel 1976). The supergranular network can be distinguished by magnetic flux in photospheric magnetograms and by emission brightness in ultraviolet (UV) spectra (Reeves 1976). Over most of the cells the magnetic field is believed to form a canopy whose height is a function of the magnetic flux density and the underlying magnetic field topology (Giovanelli 1980; Spruit 1981; Solanki 1993).

During previous and current space missions, studies of the relationship between Doppler shifts and line radiances have been used to probe the nature of these regions. The first measurements of transition region Doppler shifts were performed using the NRL normal-incidence spectrograph on board *Skylab* (Doschek et al. 1976). Gebbie et al. (1981) and Athay et al. (1983) attempted to answer the question whether Doppler shifts and cell-network structures are correlated using the Ultraviolet Spectrometer and Polarimeter (UVSP) on the *Solar Maximum Mission* (*SMM*) satellite. They obtained contradictory statistical results on the correlation between relative redshifts and bright regions in intensity for a transition region line (C IV 1548 Å). Later Dere et al. (1984) found no clear correlation between the Doppler shift in the C IV resonance lines and local intensities using the NRL High Resolution Telescope and Spectrograph (HRTS). More recently Peter (1999) found the bright regions in C IV redshifted by about 10 km s^{-1}, while the darker parts of the internetwork show no line shifts using the spectrometer SUMER (Solar Ultraviolet Measurements of Emitted Radiation) on board the *Solar and Heliospheric Observatory* (*SOHO*). Peter & Judge (1999) derived average Doppler shifts at disk center for a large number of lines accessible with SUMER to reevaluate the statistical variation of line shifts with line formation temperatures. They confirmed the first results of Doschek et al. (1976). However, they showed that lines formed at temperatures above approximately $10^{5.7}$ K are blueshifted on average. Hassler et al. (1999) indicate for Ne VIII line (770.41 Å) formed at $10^{5.8}$ K that strong outflow (blueshift) occurs along the quiet-Sun network lanes especially where lanes come together (bright network vertices) from data obtained at the north polar region using *SOHO* SUMER. Wilhelm (2000) shows by means of contour plots that the strongest blueshifts appear mostly in the dark areas in the Ne VIII line intensity in a polar region, which seems to contradict the results of Hassler et al. (1999). Aiouaz et al. (2005b) recently investigated the relation of the Ne VIII (770.41 Å) Doppler shift with the chromospheric network, and showed that the Ne VIII Doppler shifts appear statistically to be at the strongest toward the boundaries of network lanes rather than at network lanes center or cell center. This statistical result does not exclude the possibility for strong blueshifts to appear occasionally in the darkest areas in line intensity or at network vertices. In addition, one should also mention the

TABLE 1
EMISSION LINES OBSERVED WITH *SOHO* SUMER ON 1997 MARCH 7

ION	λ_{ion} (Å)	TRANSITION	log (T_{for}) (K)	BLEND		REFERENCES
				Ion	λ_{ion} (Å)	
N IV	765.15	$2s^2\ ^1S_0$–$2s\ 2p\ ^1P_1$	5.18	...	...	1
O IV	790.19	$2s^2\ 2p\ ^2P_{3/2}$–$2s\ 2p^2\ ^2D_{5/2}$	5.26	O IV	790.11	1
S V	786.50	$3s^2\ ^1S_0$–$3s\ 3p\ ^1P_1$	5.26	...	...	2
O V	760.45	$2s\ 2p\ ^3P_2$–$2p^2\ ^3P_2$	5.40	O V	760.21	1
Ne VIII[a]	770.41	$1s^2\ 2s\ ^2S_{1/2}$–$1s^2\ 2p\ ^2P_{3/2}$	5.80	...	...	3

NOTE.—Listed are ion name, wavelength of the line, electronic transition, and logarithm of temperature of formation.
[a] From the low corona (see results in Aiouaz et al. 2005b, 2007).
REFERENCES.—(1) Wilhelm et al. 2002; (2) Teriaca et al. 1999a; (3) Peter & Judge 1999.

numerous computational efforts made to explain these observed Doppler shifts (see the discussion by Peter & Judge 1999; see also Hansteen 1993; Teriaca et al. 1999b; Peter et al. 2004, 2006; Aiouaz et al. 2005a).

A current challenge is to understand the role played by the magnetic field in channeling plasma displacements throughout the solar atmosphere. Observations of looplike structures lead Dowdy et al. (1986) to propose a view of the solar atmosphere where a hierarchy of loops with different temperatures coexist with open magnetic funnel-shape structures within network lanes. Martin (1988) observed on video-magnetograms from the Big Bear Solar Observatory that the cancellation of intranetwork (internetwork) fields occurs with high frequency at the boundaries of the cells (network). This indicates that supergranular cell boundaries are in a state of continuous activity and variability. Axford et al. (1999) proposed a dynamic view of the supergranular network, where magnetic flux is continuously fed in from the sides by the convection, gives rise to reconnection and microflares, releases energy in form of waves and trigger plasma displacements. The convection-driven reprocessing of magnetic structures, e.g., through reconnections, is believed to play a key role in the nature of various transient small-scale phenomena such as spicules, macrospicules, microflares, bidirectional jets (also know as explosive events) (e.g., Porter et al. 1987; Shibata et al. 1992; Innes 2001; Yamauchi et al. 2005; McIntosh et al. 2007) and as the source of Alfvén waves for the solar wind (Parker 1991). Nevertheless, it is still not clear how transient small-scale phenomena fit with past and current statistical results from Doppler-shifts observations. Furthermore, the role of the magnetic field in the statistical results of Doppler-shifts observations need to be investigated. It is still not clear how the role of the magnetic field in a mostly unipolar coronal hole differs from a more balanced field in quiet-Sun regions.

In this context, studies of the plasma velocity and its fluctuations as a function of position provide crucial information on the plasma dynamics and the magnetic structures throughout the solar atmosphere. This paper present results from a large raster scan of $235'' \times 283''$ containing an equatorial coronal hole and surrounding quiet-Sun areas. This paper aims to extend to the transition region the study initiated in Aiouaz et al. (2005b) for the low corona (Ne VIII 770.41 Å). Thus readers are invited to refer to Aiouaz et al. (2005b) for further details on the observational data set (corrections) and display methods (dispersion plots). We report correlation properties between the chromospheric network and Doppler shifts from transition region lines (N IV 765.15 Å, O IV 790.19 Å, S V 786.50 Å, and O V 760.45 Å).

2. OBSERVATIONS AND DATA REDUCTION

The EUV spectrometer SUMER was used with the $1'' \times 300''$ (north-south) slit to perform the observation. The SUMER spectrograph and its first results have been described in detail in Wilhelm et al. (1995a, 1997) and Lemaire et al. (1997). The observation started on 1997 March 7 at 18 : 00 UT and ended on 1997 March 8 at 17 : 42 UT. The center of the slit was pointed at $x = 0''$ and $y = 279''$ in solar/*SOHO* disk coordinates. The observed regions on the Sun include an equatorial coronal hole (ECH) as well as surrounding quiet-Sun (QS) areas. More detailed descriptions of the data set can be found in Lemaire et al. (1999) and Aiouaz et al. (2005b).

The scan of about $235'' \times 283''$ was acquired in various transition region and coronal lines. The emission lines, among others, recorded during the scan are summarized in Table 1.

The coronal hole is defined by hand using the Ne VIII (770.41 Å) intensity image and Dopplergram. SUMER data sets were processed and corrected from spurious line shifts due to the geometric distortion of the detector image, and to thermal deformations of the instrument (see Curdt et al. 1997; Peter & Judge 1999; Aiouaz et al. 2005b). SUMER has a velocity sensitivity of $\sim$2 km s^{-1}, and even 1 km s^{-1} for strong enough lines as shown with simulation studies in Wilhelm et al. (1995b), Warren et al. (1997), and Judge et al. (1998). The different emission lines have been fitted with single-Gaussian profiles using the very robust and reliable forward-fitting technique driven by a genetic algorithm (PIKIA software) described in Charbonneau (1995).

During this observation, full-disk magnetograms with the Michelson Doppler Imager (MDI; Scherrer et al. 1995) on board *SOHO* were performed. One full-disk image was taken every 90 minutes. From the MDI series (16 full-disk images) we were able to reconstruct the magnetogram corresponding to the raster done by SUMER over 24 hr with a resolution of $\sim 2''$ (see Fig. 2, *bottom left panel*).

3. FILTERED CONTINUUM IMAGE

An intensity image of the Lyman continuum (see Fig. 1, *top left panel*) is used to outline the network at chromospheric temperatures. The continuum image is filtered to outline the main structures (network lanes, internetwork cells) while conserving the global distribution of the image (lognormal distribution). The filtered continuum image (see Fig. 1, *bottom left panel*) outline the two main populations of the image (bright network lanes, dark internetwork cells), and also conserve the transition between network and cell.

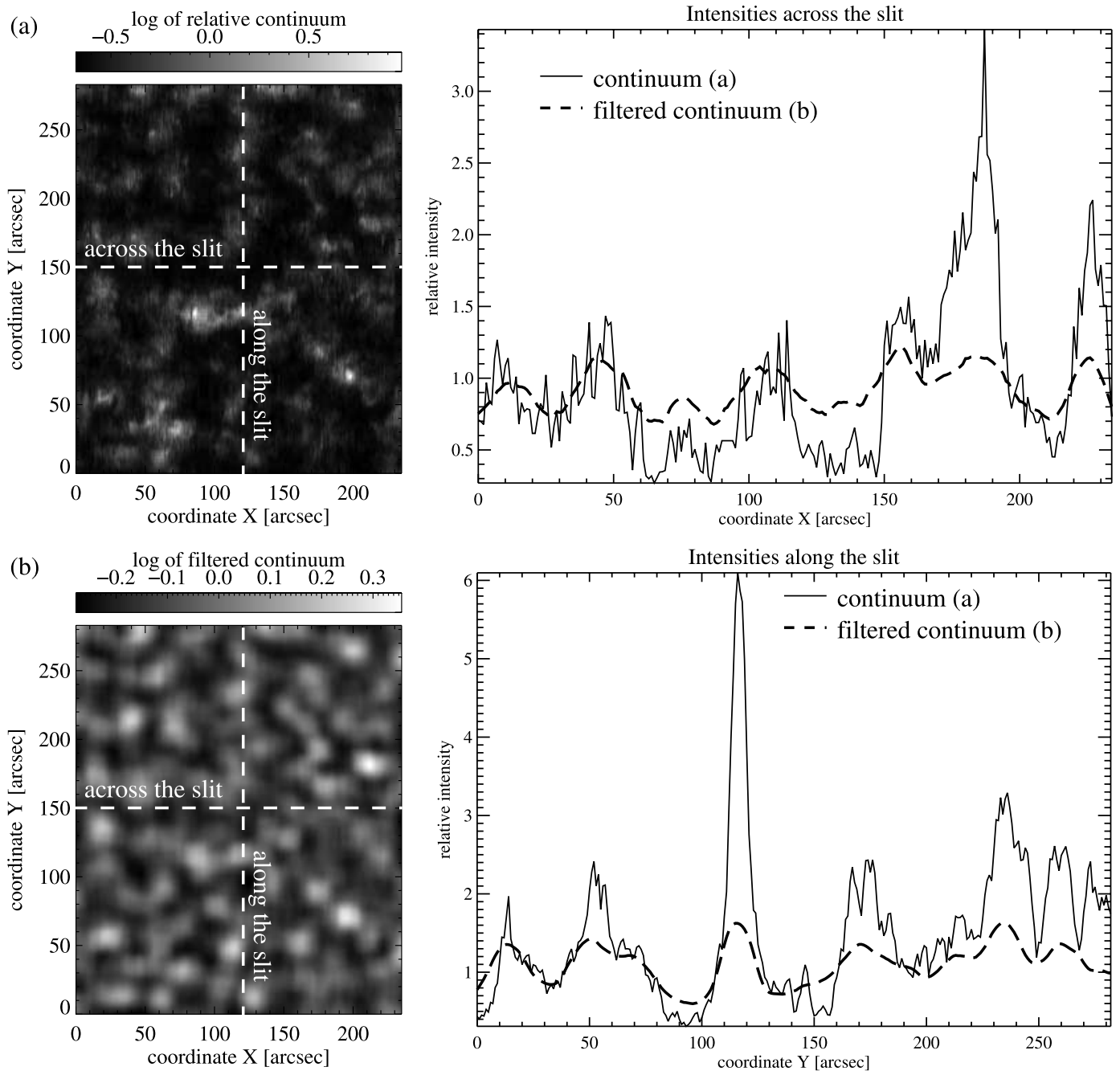

FIG. 1.—*Top left*: Lyman continuum intensity. *Bottom left*: Filtered continuum intensity. The right panels plot the continuum intensity (*solid line*) and the filtered continuum (*dashed line*) across the slit ($X = 120$) and along the slit ($Y = 150$). [*See the electronic edition of the Journal for a color version of this figure.*]

The filtering described in Aiouaz et al. (2005b) is equivalent to a bandpass filter combined with a flat-fielding (see Fig. 1, *left panels*). It consists of three steps:

1. Carry out a median filter image of a continuum image (width: supergranular scale).
2. Divide the original continuum with the median filtered image.
3. Smooth the resulting image (width: network width scale).

It reveals the network and the cell-like pattern of the supergranular convection cells, and thus allows the study of plasma velocity and its fluctuations as a function of position (i.e., the center of the network lanes, the boundary of the network lanes and the internetwork/cell interior).

4. OBSERVATIONAL RESULTS

The discussion of the observational results concentrates on two different approaches:

1. Figure 2 displays Ne VIII and N IV line shifts and their spatial relation to each other, to the magnetic field, and to the network. This highlights the plasma dynamic throughout the atmosphere and its relation to the underlying magnetic field and supergranular structure.
2. Figure 3 outlines in a statistical approach the relation between Doppler shifts of the transition region emission lines listed in Table 1 (for Ne VIII, see Aiouaz et al. 2005b, 2007) and the filtered continuum intensity. This highlights the connection between

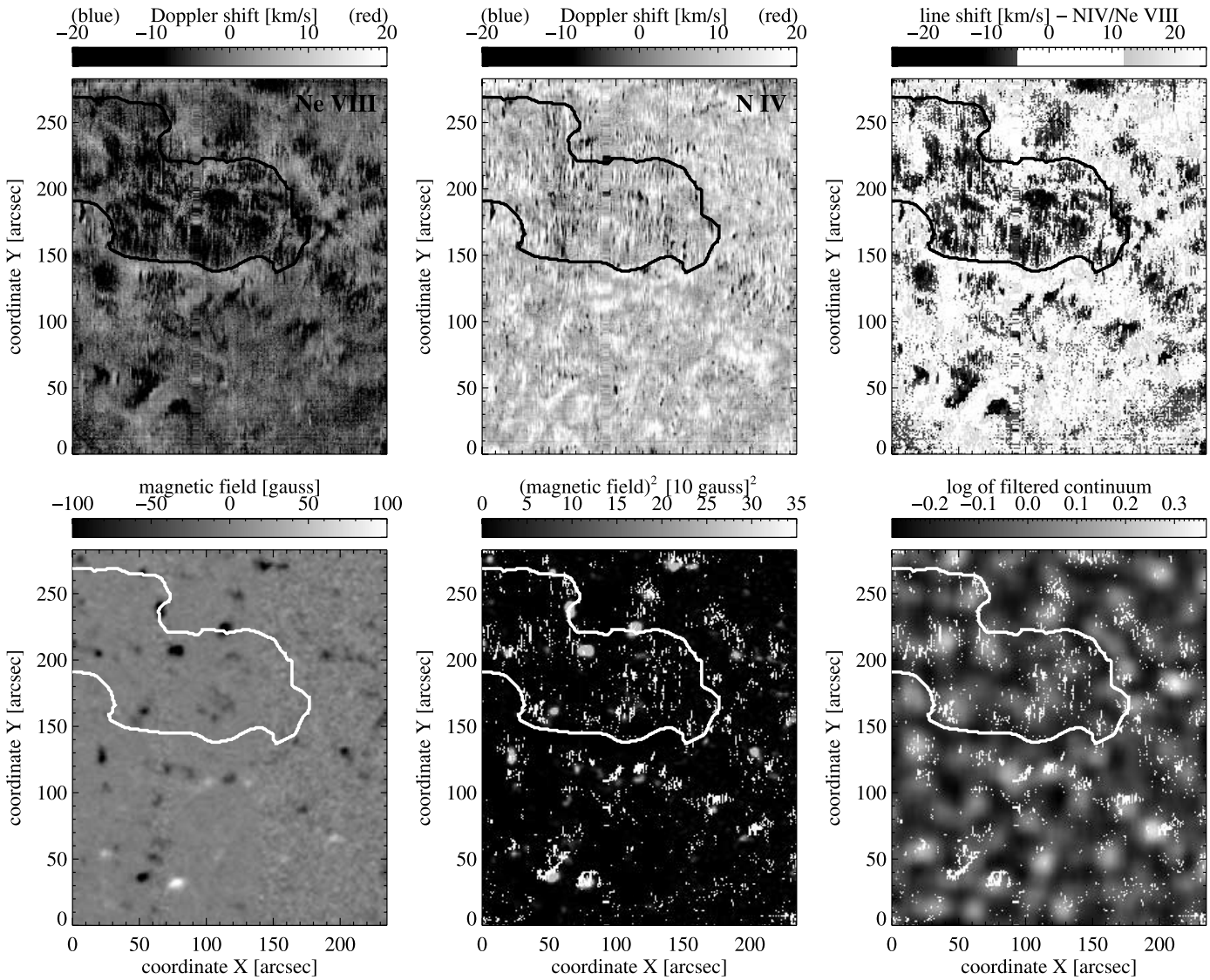

FIG. 2.—*Top panels*: Dopplergrams of the Ne VIII (*left*) and N IV (*middle*) emission lines. In the top right panel areas strongly blueshifted in the Ne VIII line and those strongly redshifted in the N IV line are put together in a N IV/Ne VIII map. These strong line shifts are defined as redshifts from the N IV line $v_D^{Ne} > 12$ km s^{-1} and blueshifts from the Ne VIII line (low corona) $v_D^{Ne} < -5$ km s^{-1}. The bottom panels show the reconstructed MDI magnetogram (*left*), the magnetic field strength (*middle*), as well as the filtered continuum image (*right*). The black areas from the top left panel are reported—in white—in the bottom panels (*middle and right*). The thick contour lines show the separation between quiet Sun and coronal hole. [*See the electronic edition of the Journal for a color version of this figure.*]

the chromospheric structure and the plasma dynamics in the transition region.

To obtain absolute Doppler shifts, the mean value of the Doppler shift of the lines over the quiet-Sun areas was set to -2.5 km s^{-1} for the Ne VIII and +9.5 km s^{-1} for the transition region lines (i.e., N IV, O IV, S V, and O V). These mean values are derived from Peter & Judge (1999). Then the Doppler shifts above the limb are approximately zero, as expected for an optically thin emission line. This method introduce uncertainties on the absolute Doppler shifts, since the mean values may vary from one emission lines to the other. Nevertheless, it is satisfactory as we are mainly interested in the relative variation of Doppler shifts over the solar surface.

The statistical study is displayed using dispersion plots as defined by Aiouaz et al. (2005b). They present the filtered continuum intensity $I_{\rm filt.cont.}$ versus emission-line Doppler shifts v_D. For each intensity bin the median value is calculated from the corresponding Doppler shift values. Each dispersion plot has been fitted with a linear function to emphasize the trend. Slope "a" is given for each fit. The standard deviation σ of the sample of N data points in the respective intensity bin is plotted as shaded areas on the dispersion plots. The standard error on each bin step $\langle\sigma\rangle/\sqrt{N}$ is kept smaller than 1 km s^{-1} ($N_{\rm min} = 20$). The sampling steps of the intensity bins were approximately 0.01, which allowed the take in account of maximum data points while fulfilling the previously described requirement on the standard error.

4.1. *Dopplergrams and Strong Line Shifts*

The top panels in Figure 2 show the Dopplergrams of the Ne VIII (*left*) and N IV (*middle*) emission lines. The top right panel shows the areas strongly blueshifted in the Ne VIII line and those strongly redshifted in the N IV line *together* (N IV/Ne VIII map). These strong line shifts are defined as redshifts from the transition region $v_D^{TR} > 12$ km s^{-1} and blueshifts from the Ne VIII line (low corona) $v_D^{Ne} < -5$ km s^{-1}. These threshold values are the absolute mean values derived from Peter & Judge (1999), i.e., 9.5 km s^{-1} for TR and -2.5 km s^{-1} for Ne VIII, plus 2.5 km s^{-1} for the TR, minus 2.5 km s^{-1} for the Ne VIII. The value 2.5 km s^{-1}

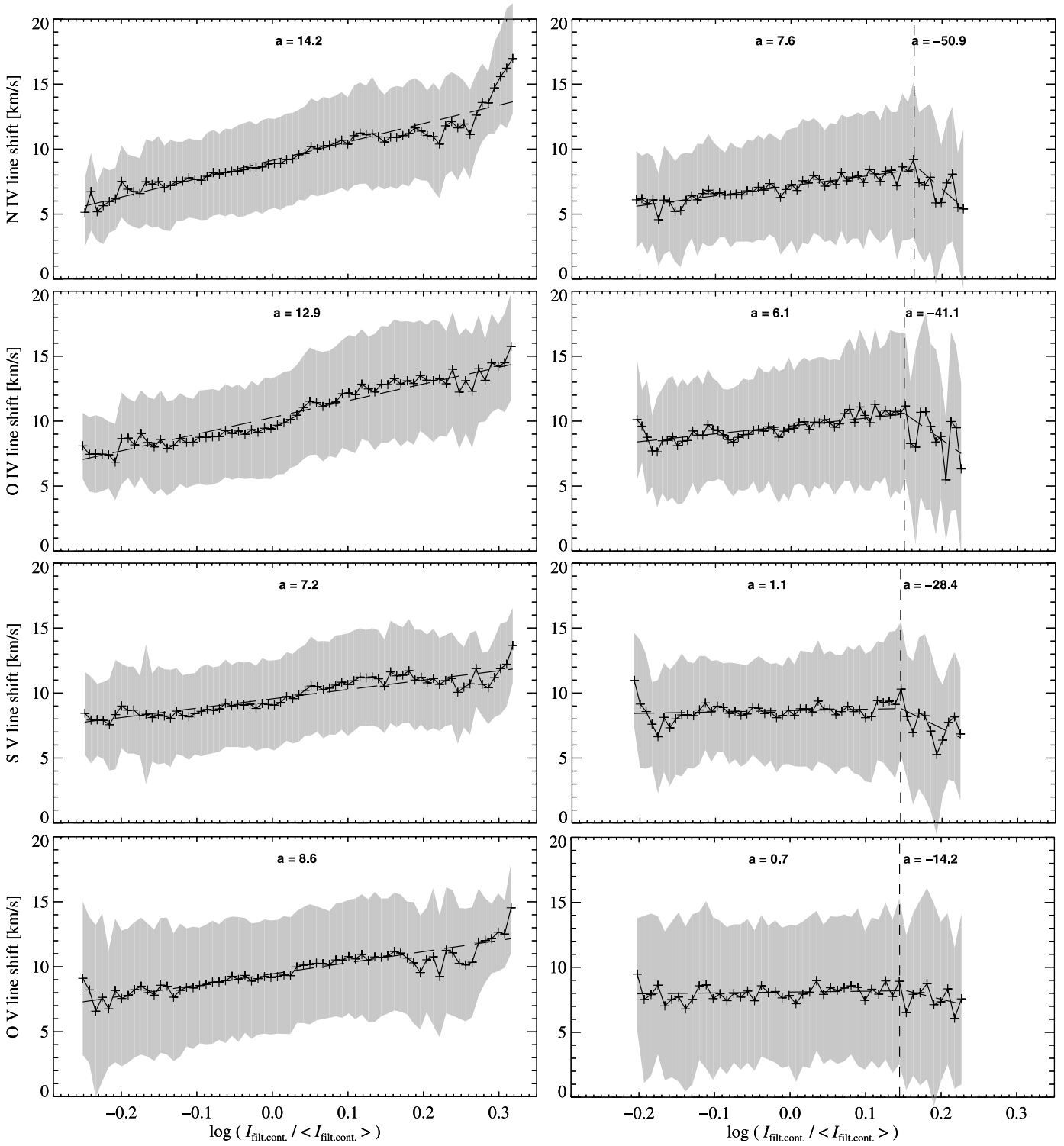

FIG. 3.—Dispersion plots showing the relation between filtered continuum intensity and transition region Doppler shift, in solid lines. The dispersion plots are fitted by linear fits in long dashed lines, where *a* is slope of the fit. The left column shows quiet-Sun data, the right column coronal hole data. The standard deviation of the median value is represented by the shaded areas. The vertical long-dashed lines show the position in the dispersion plot where the maximum Doppler shift is reached (for CH only).

is approximately half of the mean absolute deviation of the transition region Dopplergrams. The white color in the N IV/Ne VIII map (*top right panel*) shows areas that do not fulfill either of the two criteria ($v_D^{TR} > 12$ km s^{-1}, $v_D^{Ne} < -5$ km s^{-1}). The black color shows areas which fulfill both conditions, areas with bidirectional flows. The bottom panels in Figure 2 show the reconstructed MDI magnetogram (*left*), the magnetic field strength (*middle*), as well as the filtered continuum image (*right*). The black areas (bidirectional flows) from the top right panel are overplotted (*in white*) in the bottom panels (*middle and right*). The thick contour lines in Figure 2 shows the boundary between QS and CH.

Figure 2 points out the relation between plasma motions flowing in different directions (red- and blueshifts [inflow and outflow), at different atmospheric layers (TR/corona), and their relation

TABLE 2
Emission Lines and Doppler Shifts

Ion	$\log(T_{for})$ (K)	$\langle v_D\rangle_{QS} - \langle v_D\rangle_{CH}$ (km s^{-1})	Strong v_D[a] (%)		Bidirectional v_D[a]		Trend "a"[b]	
			QS	CH	QS	CH	QS	CH
N IV	5.18	2.1	30.1	19.6	8.9	10.0	14.2	7.2, −50.9
O IV	5.26	0.6	31.7	28.7	10.0	13.6	12.9	6.1, −41.1
S V	5.26	0.9	30.0	26.0	9.5	12.6	7.2	1.1, −28.4
O V	5.40	1.5	32.7	28.2	9.5	13.7	8.6	0.7, −14.2
Ne VIII[c]	5.80	2.3	22.5	48.2	...	...	...	...

Notes.—Listed are ion name, logarithm of temperature of formation (see references Table 1), difference of the median Doppler shift between quiet Sun $\langle v_D\rangle_{QS}$ and coronal hole $\langle v_D\rangle_{CH}$, percentage of strong line-shifts ($v_D^{TR} > 12$ km s^{-1}) for the transition region lines and ($v_D^{Ne} < -5$ km s^{-1}) for the Ne VIII line, percentage of bidirectional flows among the strong flows ($v_D^{TR} > 12$ and $v_D^{Ne} < -5$)/($v_D^{TR} > 12$ or $v_D^{Ne} < -5$), and trend "a" of the linear fit in the dispersion plots.

[a] From Fig. 2,

[b] From Fig. 3

[c] From the low corona (see results in Aiouaz et al. 2005b, 2007).

to the underlying magnetic field and supergranular structures. The top panels in Figure 2 clearly show more blueshifts in the CH than in the QS for the Ne VIII line and also for the TR emission lines listed in Table 1. The differences of the median Doppler shifts between QS and CH regions are 2.1, 0.6, 0.9, 1.5, and 2.3 km s^{-1} for the N IV, O IV, S V, O V, and Ne VIII emission lines, respectively (see third column in Table 2). These results are in agreement with a recent study by Xia et al. (2004). When compared with the filtered continuum intensity on the bottom right panel, it appears clearly that the strongest line shifts in Ne VIII and N IV come mainly from the network lanes. In addition, the top left panel (N IV/Ne VIII map) shows that strong blueshifts and strong redshifts fit spatially together in a puzzle-like pattern within the network lanes. Nevertheless, strong blueshifts and strong redshifts do overlap (*black areas*), and present regions with bidirectional flows. These overlaps represent only a small percentage of the total amount strong line shifts. Table 2 reports percentages of strong line-shifts (fourth and fifth column), percentage of bidirectional flows among the strong line-shifts (sixth and seventh column), in the quiet Sun and coronal hole separately. These quantitative results are presented not only for the N IV/Ne VIII map but also the other transition region lines (O IV/Ne VIII, S V/Ne VIII, O V/Ne VIII). The results in Table 2 indicate that the overlap of the strong red/blueshifts (bidirectional flows) are systematically more numerous in the coronal hole than in the quiet Sun. Furthermore, the bottom panels shows that these overlaps happen almost systematically close or even around magnetic field concentrations but *not* directly above them (*middle panel*). They also appear mostly at the boundaries of the network lanes (*right panel*).

4.2. *Doppler Shift versus Filtered Continuum Intensity*

Figure 3 shows the dispersion plots presenting Doppler shifts as a function of the filtered continuum intensity (FCI). The left column describes data from the quiet Sun and the right column data from the coronal hole.

The dispersion plots show the same general behavior independently from the TR line considered. For the quiet-Sun part, the dispersion plots show a clear increase of redshift with increasing FCI. For the coronal hole, two different trends are observed. The main part of the dispersion plot shows a clear increase of the redshift with increasing FCI, while in the high-intensity range the redshift decreases with increasing intensity. Even though the decrease of redshift with FCI is significant, the median values of Doppler shifts appear more scattered than in the main part of the plot. This places statistically the maximum redshifts toward the network boundaries for the CH. All considered emission lines in Figure 3 show the same general behavior; nevertheless, one can notice that the trends of the dispersion plots seems to decrease with temperature (see also Table 2). The strongest trends appear for the "coolest" considered transition region line (N IV, 765.15 Å). While the weakest trends appear for the S V line for the quiet Sun and for the O V line for the coronal hole.

5. DISCUSSION

5.1. *Transition Region Flows*

The results of the dispersion plots in Figure 3 are in agreement with previous works done by Gebbie et al. (1981); Peter (1999) for the QS. The strong redshifts in the transition region lines appear statistically in the network lanes. Nevertheless, Figure 3 clearly show for the first time the difference of behavior between QS (*left panels*) and CH (*right panels*). A new result is that in the CH part, the maximum redshifts appear toward network lane boundaries, as opposed to the QS where the maximum redshifts clearly appear toward network lane center. This difference must be symptomatic of the role played by the magnetic field in plasma motions. It is commonly accepted that coronal holes present stronger net flux than quiet Sun (Bohlin 1977), being predominantly of one polarity. This property lead to differences in the magnetic field structure and in the expansion of the network throughout the atmosphere (Aiouaz & Rast 2006).

The distinctions between quiet Sun and the coronal hole remains similar throughout the different transition region emission lines, i.e., throughout the different atomic physic processes exciting the different electronic transitions. This indicates that the observed pattern in the dispersion plots has a thermodynamic (macroscopic) origin as opposed to an atomic physic (microscopic) origin. Nevertheless, the dispersion plots of the different transition region lines shows different values for the trends. One can indeed notice that the absolute values of trend "a" of the fit seem to decrease with increasing formation temperature. However, the range of temperature formations available in this study is presently not sufficient to interpret these trend variations.

5.2. *Bidirectional Flows*

Figure 2 presents new views of the complementary pattern of the Doppler shifts in the transition region and low corona. Most of the strong Doppler shifts in the N IV/Ne VIII map (*top right panel*) appears to coincide spatially in a puzzle-like pattern within the network lanes. Although a small percentage of the

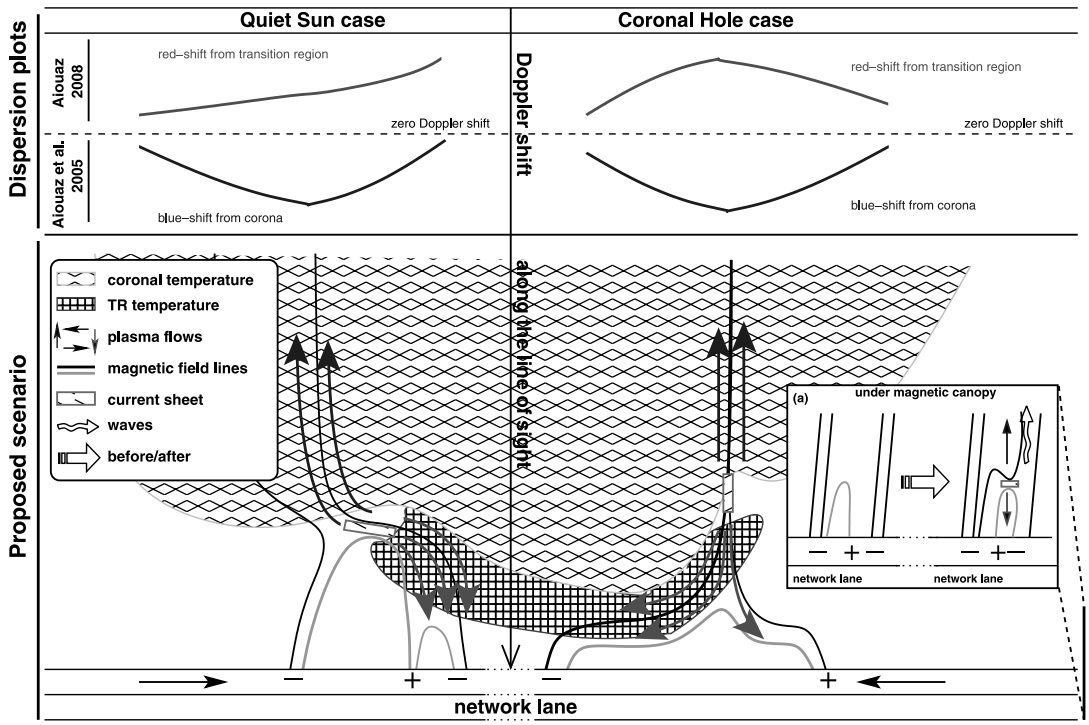

FIG. 4.—Sketch of the structure of the transition region. The bottom part presents the proposed scenarios for the quiet Sun and coronal hole. The top part shows the expected dispersion plots from the corresponding scenario-like events. The sketch is discussed in detail in § 6. [*See the electronic edition of the Journal for a color version of this figure.*]

area presents bidirectional flows (see Table 2). The bidirectional flows seem to be systematically related to magnetic field concentrations. These results indicate that the magnetic field plays a major role in driving the flows in the transition region and in the corona. One possible explanation for bidirectional flows triggered by the magnetic field is reconnection events, which drive flows in opposite directions due to the local reprocessing of the magnetic field. These driven flows are required to have a line of sight component in order to be observable by a spectrometer like *SOHO* SUMER.

The bidirectional flows appear mostly at network boundaries, and are more frequent in the coronal hole than in the quiet Sun (see Table 2). This result supports the statistical result presented in Figure 3 where the maximum redshifts appears at intermediate intensities in the coronal hole.

6. INTERPRETATION

6.1. *Reconnections at Network Boundaries*

The new results discussed in § 5 reveal the main ingredients and a possible trigger for the plasma motion in the TR and low corona. It is thus possible to suggest a coherent scenario to explain the different observed patterns. Figure 4 presents scenarios to interpret the current and past EUV observations of Doppler-shifts variations in QS and CH. The sketch represent in the bottom panels an idealized view of the most common scenario for the QS (*left part*) and CH (*right part*). The top panels show the corresponding statistical results to expect from a scenario as depicted in the bottom panels. The case of the QS (*left part*) in Figure 4 is different from the CH, even though the trigger and main ingredients remain the same in both cases. The idealized structure of the network magnetic field in the bottom part of Figure 4 is a funnel-like structure, which expands throughout the transition region until it feels the corona. Peter (2001) pointed out that these coronal funnels can be viewed as the base of, either large coronal loops in a mostly bipolar environment (quiet-Sun case), or magnetically open structures connected to the solar wind in a mostly unipolar environment (coronal hole case). This funnel-like structure arises from force balance and cannot reasonably be expected to be avoided. Figure 4 presents, however, a simplified view of the magnetic field structure in the supergranular network (Aiouaz & Rast 2006); nevertheless, it is satisfactory as illustration. This scenario involves two main ingredients to explain the line-shift behaviors, the magnetic field structure and line-of-sight projection. It proposes a single trigger, reconnections at network boundaries driven by convection. As the photospheric footpoints of the field lines move toward the network, current sheets are formed at the interface of oppositely directed flux tubes, magnetic field reconnects and magnetic energy is released in the process. The timescale and the amount of energy at which magnetic energy is converted into heat and flow energy, depends mainly on the diffusivity, plasma velocity, and magnetic field strength at the reconnection site (see Priest 1982 and references within). The suggested reconnection events release enough energy to trigger detectable plasma motion. Although they do not change significantly the magnetic field topology nor the global temperature stratification of the network structure. Thus these reconnections significantly differentiate themselves from large flarelike events. At these heights and temperatures the plasma is dominated by the magnetic field (low-β plasma). At the reconnection site the plasma moves away and/or across mostly horizontal field (magnetic canopy) in a bidirectional flow along the magnetic field lines. The plasma motion appears as line shift in EUV when observed with a spectrometer like *SOHO* SUMER. Doppler shift is a function of the plasma velocity projected along the line of sight. Therefore, for a given plasma velocity, Doppler shifts appear maximum wherever the field lines driving the plasma is parallel to the line of sight. Perpendicular

motion to the line of sight does not appear in observation for any given plasma velocity. The structural difference between the quiet Sun and the coronal hole is based on two commonly accepted properties:

1. The thermal pressure is lower in the coronal hole than in the quiet Sun (Withbroe & Noyes 1977).
2. The magnetic field is more unipolar in the coronal hole and the net magnetic flux is stronger compare to the quiet Sun (Bohlin 1977).

These properties lead one to consider different expansion rate for the magnetic field, and different predominant locations for reconnections along the funnel-shape magnetic field lines. While for the quiet Sun the predominant reconnection site is assumed to be at the location where the magnetic field is perpendicular to the line of sight. The coronal hole case scenario follow the assumption that the reconnection sites are located where the field is parallel to the line of sight. Thus, in the quiet-Sun case, the strongest shifts appear when the plasma flow reaches the mostly vertical magnetic field lines, i.e., toward the boundary of the magnetic field concentration for the upward moving plasma, toward the center of the magnetic field concentration for downward moving plasma. One should thus expect a complementary pattern (puzzle-like) for the blueshifts and redshifts of the TR/corona map as presented in the top left panel in Figure 2. In the coronal hole, the magnetic field lines at reconnection sites are parallel to the line of sight. This implies that the redshifted and the blueshifted emission appears at the same location, the reconnection site. The signature of these spatially overlapping blue- and redshifts appears as bidirectional flows as presented with the black pixels in the top left panel in Figure 2.

The scenario presented in Figure 4 conciliates the phenomenological results of Figure 2 and the statistical results of Figure 3 and Aiouaz et al. (2005b, 2007).

6.2. *Phenomenological versus Statistical*

The relentless reprocessing of magnetic structures has lead to the idea that small magnetic flux elements contribute significantly through reconnection to the energy balance in the solar atmosphere and might even be the prime energy source for sustaining the solar corona (Porter et al. 1987; Martin 1988; Parker 1991; Axford et al. 1999; Priest & Schrijver 1999; Priest et al. 2002). Transient events such as explosive events (EEs) are traditionally separated from statistical results from plasma motions in the solar atmosphere. Unfortunately, detection and classification of these various events is driven as much by instrumental limitations and observational techniques as by physical processes (Harrison et al. 2003). The next section thus aims to outline common characteristics between transient events properties and statistical results of Doppler-shifts observations. The basic goal is to clarify the fundamental physical processes occurring in the QS and CH to aid and improve future modeling.

6.2.1. *Explosive Events and Microflares*

Bidirectional jets (also know as EEs) were first identified by Brueckner & Bartoe (1983) in spectra from the NRL High Resolution Telescope and Spectrograph (HRTS). Bidirectional jets are observationally defined by Doppler shifts rather than brightenings in UV lines, even though they are routinely associated to microflares (Porter et al. 1987; Rabin & Dowdy 1992). They have a scale of about 1500–4000 km, high-velocity wings at about ± 100–150 km s^{-1} in their line profiles, a mean lifetime of 60 s, and a frequency around 500 s^{-1} (Innes et al. 1997; Innes 2001). For velocities below 50 km s^{-1} these events become increasingly harder to detect. Furthermore, Dere et al. (1989) found no preferred direction for bidirectional jets; thus their detection is limited to those aligned to the line of sight. Axford et al. (1999; first published by Axford & McKenzie 1992) suggested that network microflares release a spectrum of high-frequency waves, which heat the corona by cyclotron absorption (see Fig. 4*a*).

6.2.2. *Spicules and Macrospicules*

Solar spicules are rapidly evolving jetlike structures from the chromosphere upward and are traditionally observed on the limb in cool chromospheric lines such as Hα (see Beckers 1968, 1972). They are reported to be more numerous, and slightly taller at polar coronal holes (e.g., Bohlin et al. 1975; Moore et al. 1977). They are also seen in EUV lines showing a bigger size and a longer lifetime and are named, because of their size, macrospicules (Bohlin et al. 1975). Spicules studies are observationally limited, and many questions about their properties and origin are not yet answered. There are strong debates as to whether Hα and EUV spicules are connected, and whether they are due to propagating waves or to magnetic reconnection (see Sterling 2000). Recent study by Yamauchi et al. (2004) show that Hα macrospicule characteristics observed on the limb fits magnetic reconnection models (e.g., Shibata et al. 1992). Yamauchi et al. (2005) show that the on-disk counterparts of the Hα macrospicules seat at the boundaries of the magnetic network lanes and results most likely from explosive events.

6.2.3. *Common Properties*

The present study does not provide direct information for current debates on EEs and spicules. Nevertheless, previously mentioned studies support convection-driven reconnection models, and one can at least wonder whether the proposed scenarios (see Fig. 4) in the current study does apply to a broader range of events such as EEs and spicules.

The bidirectional flows presented in this study are defined by opposite sign Doppler shifts at two different temperature layers but at the same time and spatial location. These line shifts are commonly observed in TR and coronal emission lines. TR emission lines show typically redshifts of about 15 km s^{-1} on average. Coronal emission lines present blueshifts of about -5 km s^{-1} over the full disk (see Peter 1999).

These bidirectional plasma motions share common properties with previously presented transient events. They appear to be primarily network phenomena. Porter & Dere (1991) show that EEs occur at boundaries of supergranular convective cells and rather on the edges of unipolar fields. This property on the location is common to bidirectional flows which seem to appear systematically close to magnetic field concentrations but *not* directly above them. Furthermore, even though there is some controversy on where exactly the EEs occur in the solar atmosphere, i.e., where the neutral points reconnections are located. They seems mostly confined to TR temperatures (see Innes 2001). It is, at the least, interesting to note that the sign reversal of average Doppler shifts found by Peter & Judge (1999) appears also at transition region temperature at approximately $10^{5.7}$ K.

7. CONCLUSION

The main goal of this paper was to determine correlations between the chromospheric network and the N IV (765.15 Å), O IV (790.19 Å), S V (786.50 Å), and O V (760.45 Å) Doppler shifts in quiet Sun and in coronal hole part, with special regard to the relation to the magnetic field. The SUMER data presented above show clearly for the first time that the maximum inflow appear in the network center for the quiet-Sun part, but toward network

boundaries for the coronal hole. These results are consistent with previous results by Peter (1999) for the quiet Sun.

Furthermore, this study establishes the existence of dominant puzzle-like pattern of the strong blueshifts in the low corona and strong redshifts in the transition region. Bidirectional flows, i.e., strong redshifts in the transition region and strong blueshifts in the corona at the same location, appear to be a minority. Nevertheless, these bidirectional flows appear almost systematically at or even around strong magnetic field concentrations. In addition, they seems more numerous in the coronal hole than in the quiet Sun.

Based on these results a coherent scenario is proposed that involves a single driver: continuous reconnection at supergranular network boundaries. This scenario explain the differences observed between quiet Sun and coronal hole in the relation between Doppler shifts and network structures. Furthermore, it provides the main ingredients to explain the puzzle-like pattern between the strong blueshifts in the low corona and strong redshifts in the transition region. This scenario helps to understand 20 years of Doppler-shifts observation of the transition region and low corona in the quiet Sun and coronal hole.

This study motivates further work on correlations between hotter and cooler lines and has serious implications on transition region and coronal funnel modeling, as well as on our understanding transient events, heating of the solar corona, and acceleration of the solar wind.

I would like to thank Phil Judge for the careful reading of the manuscript and for very helpful comments and suggestions. The SUMER project is financially supported by DLR, CNES, NASA, and the PRODEX project (Swiss contribution). SUMER and MDI are part of *SOHO*, the *Solar and Heliospheric Observatory* of ESA and NASA.

REFERENCES

Aiouaz, T., Peter, H., & Keppens, R. 2005a, A&A, 442, L35
Aiouaz, T., Peter, H., & Lemaire, P. 2005b, A&A, 435, 713
———. 2007, A&A, 466, 689
Aiouaz, T., & Rast, M. 2006, ApJ, 647, L183
Athay, R. G., Gurman, J. B., Henze, W., & Shine, R. A. 1983, ApJ, 265, 519
Axford, W. I., & McKenzie, J. F. 1992, in Proc. 3rd COSPAR Colloq., Solar Wind Seven Colloquium, ed. E. Marsch & R. Schwenn (Oxford: Pergamon), 1
Axford, W. I., McKenzie, J. F., Sukhorukova, G. V., Banaszkiewicz, M., Czechowski, A., & Ratkiewicz, R. 1999, Space Sci. Rev., 87, 25
Beckers, J. M. 1968, Sol. Phys., 3, 367
———. 2007, 1972, ARA&A, 10, 73
Bohlin, J. D. 1977, Sol. Phys., 51, 377
Bohlin, J. D., Vogel, S. N., Purcell, J. D., Sheeley, Jr., N. R., Tousey, R., & Vanhoosier, M. E. 1975, ApJ, 197, L133
Brueckner, G. E., & Bartoe, J.-D. F. 1983, ApJ, 272, 329
Charbonneau, P. 1995, ApJS, 101, 309
Curdt, W., Kucera, A., Rybak, J., Schühle, U., & Wöhl, H. 1997, in The Corona and Solar Wind Near Minimum Activity, ed. A. Wilson (ESA SP-404; Noordwijk: ESA), 307
Dere, K. P., Bartoe, J.-D. F., & Brueckner, G. E. 1984, ApJ, 281, 870
———. 1989, Sol. Phys., 123, 41
Doschek, G. A., Bohlin, J. D., & Feldman, U. 1976, ApJ, 205, L177
Dowdy, J. F., Jr., Rabin, D., & Moore, R. L. 1986, Sol. Phys., 105, 35
Gabriel, A. H. 1976, Philos. Trans. R. Soc. London A., 281, 339
Gebbie, K. B., et al. 1981, ApJ, 251, L115
Giovanelli, R. G. 1980, Sol. Phys., 68, 49
Hansteen, V. 1993, ApJ, 402, 741
Harrison, R. A., Harra, L. K., Brković, A., & Parnell, C. E. 2003, A&A, 409, 755
Hassler, D. M., Dammasch, I. E., Lemaire, P., Brekke, P., Curdt, W., Mason, H. E., Vial, J.-C., & Wilhelm, K. 1999, Science, 283, 810
Innes, D. E. 2001, A&A, 378, 1067
Innes, D. E., Inhester, B., Axford, W. I., & Willhelm, K. 1997, Nature, 386, 811
Judge, P. G., Hansteen, V., Wikstol, O., Wilhelm, K., Schuehle, U., & Moran, T. 1998, ApJ, 502, 981
Leighton, R. B., Noyes, R. W., & Simon, G. W. 1962, ApJ, 135, 474
Lemaire, P., Bocchialini, K., Aletti, V., Hassler, D., & Wilhelm, K. 1999, Space Sci. Rev., 87, 249
Lemaire, P., et al. 1997, Sol. Phys., 170, 105
Martin, S. F. 1988, Sol. Phys., 117, 243
McIntosh, S. W., Davey, A. R., Hassler, D. M., Armstrong, J. D., Curdt, W., Wilhelm, K., & Lin, G. 2007, ApJ, 654, 650
Moore, R. L., Tang, F., Bohlin, J. D., & Golub, L. 1977, ApJ, 218, 286
Parker, E. N. 1991, ApJ, 372, 719
Peter, H. 1999, ApJ, 516, 490
———. 2001, A&A, 374, 1108
Peter, H., Gudiksen, B. V., & Nordlund, Å. 2004, ApJ, 617, L85
———. 2006, ApJ, 638, 1086
Peter, H., & Judge, P. G. 1999, ApJ, 522, 1148
Porter, J. G., & Dere, K. P. 1991, ApJ, 370, 775
Porter, J. G., Moore, R. L., Reichmann, E. J., Engvold, O., & Harvey, K. L. 1987, ApJ, 323, 380
Priest, E. 1982, Solar Magnetohydrodynamics (Geophys. Astrophys. Monogr. 21; Dordrecht: Reidel)
Priest, E. R., Heyvaerts, J. F., & Title, A. M. 2002, ApJ, 576, 533
Priest, E. R., & Schrijver, C. J. 1999, Sol. Phys., 190, 1
Rabin, D., & Dowdy, J. F., Jr. 1992, ApJ, 398, 665
Reeves, E. 1976, Sol. Phys., 46, 53
Scherrer, P. H., et al. 1995, Sol. Phys., 162, 129
Shibata, K., et al. 1992, PASJ, 44, L173
Solanki, S. K. 1993, Space Sci. Rev., 63, 1
Spruit, H. C. 1981, in The Sun as a Star, ed. S. Jordan (Washington: NASA), 385
Sterling, A. C. 2000, Sol. Phys., 196, 79
Teriaca, L., Banerjee, D., & Doyle, J. G. 1999a, A&A, 349, 636
Teriaca, L., Doyle, J. G., Erdélyi, R., & Sarro, L. M. 1999b, A&A, 352, L99
Warren, H. P., Mariska, J. T., & Wilhelm, K. 1997, ApJ, 490, L187
Wilhelm, K. 2000, A&A, 360, 351
Wilhelm, K., Inhester, B., & Newmark, J. S. 2002, A&A, 382, 328
Wilhelm, K., et al. 1995a, Sol. Phys., 162, 189
———. 1995b, Proc. SPIE, 2517, 2
———. 1997, Sol. Phys., 170, 75
Withbroe, G. L., & Noyes, R. W. 1977, ARA&A, 15, 363
Xia, L. D., Marsch, E., & Wilhelm, K. 2004, A&A, 424, 1025
Yamauchi, Y., Moore, R. L., Suess, S. T., Wang, H., & Sakurai, T. 2004, ApJ, 605, 511
Yamauchi, Y., Wang, H., Jiang, Y., Schwadron, N., & Moore, R. L. 2005, ApJ, 629, 572